GEOPHYSICS, VOL. 75, NO. 6 (NOVEMBER-DECEMBER 2010); P. SA105–SA115, 6 FIGS.
10.1190/1.3494083

Nonlinear extended images via image-domain interferometry

Ivan Vasconcelos[1,3], Paul Sava[2], and Huub Douma[3]

ABSTRACT

Wave-equation, finite-frequency imaging and inversion still face many challenges in addressing the inversion of highly complex velocity models as well as in dealing with nonlinear imaging (e.g., migration of multiples, amplitude-preserving migration). Extended images (EIs) are particularly important for designing image-domain objective functions aimed at addressing standing issues in seismic imaging, such as two-way migration velocity inversion or imaging/inversion using multiples. General one- and two-way representations for scattered wavefields can describe and analyze EIs obtained in wave-equation imaging. We have developed a formulation that explicitly connects the wavefield correlations done in seismic imaging with the theory and practice of seismic interferometry. In light of this connection, we define EIs as locally scattered fields reconstructed by model-dependent, image-domain interferometry. Because they incorporate the same one- and two-way scattering representations used for seismic interferometry, the reciprocity-based EIs can in principle account for all possible nonlinear effects in the imaging process, i.e., migration of multiples and amplitude corrections. In this case, the practice of two-way imaging departs considerably from the one-way approach. We have studied the differences between these approaches in the context of nonlinear imaging, analyzing the differences in the wavefield extrapolation steps as well as in imposing the extended imaging conditions. When invoking single-scattering effects and ignoring amplitude effects in generating EIs, the one- and two-way approaches become essentially the same as those used in today's migration practice, with the straightforward addition of space and time lags in the correlation-based imaging condition. Our formal description of the EIs and the insight that they are scattered fields in the image domain may be useful in further development of imaging and inversion methods in the context of linear, migration-based velocity inversion or in more sophisticated image-domain nonlinear inverse scattering approaches.

INTRODUCTION

Seismic imaging and model estimation still present daunting challenges to the geophysical community when it comes to dealing with areas of high structural complexity or using nonlinear scattering present in the data (e.g., in the form of multiples or amplitude effects). One avenue to address these challenges is full-waveform inversion methods (e.g., Tarantola, 1984; Pratt, 1999; Sirgue and Pratt, 2004; Plessix, 2006; Tape et al., 2009; Zhu et al., 2009). These methods operate by finding models that best fit the recorded data. Although in principle they are well suited to handle nonlinear scattering effects in the data, waveform inversion methods are notoriously ill posed in terms of their sensitivity to the choice of starting models.

An alternative to deal with the ill-posedness of data-domain nonlinear inversions such as waveform inversion or inverse scattering approaches (e.g., Rose et al., 1985; Budreck and Rose, 1990; Weglein et al., 2003) is to set up the nonlinear inverse problem in the subsurface image domain (e.g., de Hoop et al., 2006; Symes, 2008, 2009). These approaches demonstrate their potential for linear wave-equation, migration-based velocity inversion (e.g., Chauris, 2000; Mulder and ten Kroode, 2002; Sava and Biondi, 2004). A key element necessary for image-domain, finite-frequency inversion methods is the analysis of subsurface image gathers. Extended images (EIs; see Sava and Vasconcelos, 2010), as we describe in this paper, are an extension of traditional subsurface-domain image gathers. As such, our objective is to provide formalism and insight for one- and two-way EIs that serve as the basis for developing image-domain inversion approaches.

Most wave-equation-based imaging methods rely on crosscorrelating source and receiver wavefields to invoke the zero-time-lag

Manuscript received by the Editor 15 February 2010; revised manuscript received 18 May 2010; published online 3 November 2010.
[1]University of Edinburgh, School of GeoSciences, Edinburgh, U. K. E-mail: ivasconc@gmail.com.
[2]Colorado School of Mines, Center for Wave Phenomena, Golden, Colorado, U.S.A. E-mail: psava@mines.edu.
[3]ION Geophysical, GXT Imaging Solutions, Princeton, New Jersey, U.S.A. E-mail: huub.douma@iongeo.com.

and zero-space-lag imaging condition (e.g., Claerbout, 1971, 1985). This imaging condition has been extended by correlating wavefields with nonzero lags in the spatial coordinates (Sava and Fomel, 2003). This allows us, for example, to study the dependence of the image gathers on the velocity used in wave-equation-based imaging. Besides allowing for lags in the spatial coordinates when calculating field correlations, one can also study the behavior of images after including nonzero lags in the time variable (Rickett and Sava, 2002; Sava and Fomel, 2006; Sava and Vasconcelos, 2010). We refer to the images obtained using nonzero lags in the spatial and time variables as EIs.

In seismic interferometry, crosscorrelating wavefields received at two receivers allows us to extract the response between these receivers as if one of them acts as a source (e.g., Claerbout, 1968; Fink, 1997; Rickett and Claerbout, 1999; Weaver and Lobkis, 2001; Campillo and Paul, 2003; Schuster et al., 2004; Wapenaar, 2004; Curtis et al., 2006; Wapenaar et al., 2006, and references therein; Wapenaar et al., 2010). Representation theorems for the scattered field traveling from one point inside the medium to another can be found using scattering reciprocity relations (Wapenaar, 2007; Wapenaar et al., 2008; Vasconcelos et al., 2009b). These theorems contain surface integrals such as those in seismic interferometry.

An image of a scatterer can be obtained by collapsing the recorded scattered wavefield onto the scatterer location, so this formulation based on scattering representations can help interpret the imaging condition in the context of seismic interferometry (Vasconcelos, 2008): the image is the zero-time, scattered-wave response generated by zero-offset pseudoexperiments in the image domain. Here we expand on this notion of image-domain interferometry and show that the representation theorems for the scattered field allow the extended images to be described as scattered wavefields that are excited and recorded in the image domain. We demonstrate this for the one-way and two-way wave-equation formulations.

Explicitly defining EIs from exact one- and two-way scattering reciprocity theorems is the essence of our work, but the integral representations in seismic interferometry are not entirely new to seismic imaging. Esmersoy and Oristaglio (1988) and Oristaglio (1989) use reciprocity integrals to formulate wavefield extrapolation for double focusing in reverse-time migration algorithms, and de Hoop and de Hoop (1999) utilize general reciprocity relations to describe the data redatuming for imaging general acoustic, elastic, and electromagnetic fields. In the context of linear imaging, Born-based migration/inversion reciprocity relations describe wavefield extrapolation for one-way (e.g., Wapenaar et al., 1989; Thorbecke and Berkhout, 2006) and two-way (e.g., Clayton and Stolt, 1981; Stolt and Weglein, 1985) imaging. Van Manen et al. (2006) were the first to point out the relationship between seismic interferometry and the migration resolution function, developed in detail by Thorbecke and Wapenaar (2007). Vasconcelos (2008) followed with an explicit general representation of Claerbout's (1971, 1985) imaging condition using scattering-based integral relations originally derived for seismic interferometry (Vasconcelos and Snieder, 2008; Vasconcelos et al., 2009b). More recently, Halliday and Curtis (2010) have derived the formal link between imaging by double focusing (Oristaglio, 1989) in terms of the scattering-based version of the source-receiver interferometry method by Curtis and Halliday (2010).

In this paper, we further explore the connection first established by Vasconcelos et al. (2009a) between wave-equation imaging and seismic interferometry in general scattering experiments for one-way as well as two-way propagation. We begin our discussion by defining EIs for one- and two-way imaging explicitly as space- and time-dependent subsurface scattering experiments. Next, we use reciprocity theorems for one — (Wapenaar et al., 2008) and two-way (Vasconcelos et al., 2009b) imaging to formally describe the extended imaging conditions. We explain how to generate one- and two-way EIs in terms of wavefield extrapolation steps as well as in terms of evaluating the imaging conditions. Finally, we address computing EIs in the context of the single-scattering assumption and connect our reciprocity-based formulation to current practice in one- and two-way migrations.

DEFINING A WAVEFIELD-BASED IMAGE

Two-way extended images

An imaging condition for migration by wavefield extrapolation can be defined in terms of a scattered field G_S as (Claerbout, 1971)

$$\mathcal{I}(\mathbf{x}) = G_S(\mathbf{x},\mathbf{x},\tau = 0). \tag{1}$$

According to this definition, the conventional image $\mathcal{I}(\mathbf{x})$ can be physically thought of as a zero-offset scattered field for source and receiver coinciding at the image point $\mathbf{x}$, evaluated at zero time (i.e., at time $\tau = 0$). Waves in the subsurface travel with finite wavespeeds, so the zero-offset, scattered-wave response in equation 1 is zero when $\mathbf{x}$ is away from scatterers or interfaces, and it is finite when the image point is at a scatterer or interface. Thus, the principle of causality makes the image in equation 1 physically suitable for mapping discontinuities in the subsurface.

Based on the definition in equation 1, an EI can be defined readily by evaluating the scattered field G_S for finite source-receiver offsets and at nonzero times:

$$\mathcal{I}_e(\mathbf{x},\delta\mathbf{x},\tau) = G_S(\mathbf{x} + \delta\mathbf{x},\mathbf{x},\tau), \tag{2}$$

where $\delta\mathbf{x}$ and τ can be thought of as space and time lags, respectively. Note that equation 2 states that the extended image $\mathcal{I}_e$ corresponds to the scattered-wave response excited by a source at $\mathbf{x}$ and recorded by receivers at $\mathbf{x} + \delta\mathbf{x}$ at time τ. Because there are no real physical excitations or observations inside the subsurface, we refer to them as pseudosources and pseudoreceivers. In addition, it is possible to define other types of extended images with pseudoacquisition geometries that differ from that in equation 2. Although the $\mathcal{I}_e$ in equation 2 represents a common-source geometry, defining $\mathcal{I}_e(\mathbf{x},\delta\mathbf{x},\tau) = G_S(\mathbf{x} + \delta\mathbf{x},\mathbf{x} - \delta\mathbf{x},\tau)$ generates a common-midpoint geometry, where the conventional image point $\mathbf{x}$ lies at the midpoint between pseudosources at $\mathbf{x} - \delta\mathbf{x}$ and pseudoreceivers at $\mathbf{x} + \delta\mathbf{x}$. Figure 1 illustrates the latter.

Equations 1 and 2 identify an image as a scattered wavefield, i.e., as a space- and time-dependent object that satisfies the partial differential equation (PDE)

$$\hat{\mathcal{L}}\hat{\mathcal{I}}_e = -\mathcal{V}\hat{G}_0, \tag{3}$$

where $\hat{G}_0$ are frequency-domain Green's functions; $\hat{\mathcal{L}}(\mathbf{x})$ is a wave-equation operator, e.g., $\hat{\mathcal{L}}(\mathbf{x}) = \nabla^2 + c^{-2}(\mathbf{x})\omega^2$; and $\mathcal{V}(\mathbf{x})$ is a scattering operator, e.g., given $\hat{\mathcal{L}}_0(\mathbf{x}) = \nabla^2 + c_0^{-2}(\mathbf{x})\omega^2$, $\mathcal{V} = \hat{\mathcal{L}}(\mathbf{x}) - \hat{\mathcal{L}}_0(\mathbf{x}) = \omega^2[c^{-2}(\mathbf{x}) - c_0^{-2}(\mathbf{x})]$. Here, $c(\mathbf{x})$ and $c_0(\mathbf{x})$ pertain to the perturbed and reference subsurface wavespeed models, respectively. Also, we assume $\hat{G} = \hat{G}_0 + \hat{G}_S$, $\hat{\mathcal{L}}_0\hat{G}_0 = \delta(\mathbf{x} - \mathbf{x}_s)$ and $\hat{\mathcal{L}}\hat{G} = \delta(\mathbf{x} - \mathbf{x}_s)$, where $\mathbf{x}_s$ is some source position. It follows from the definition of $\mathcal{V}$ that $\mathcal{L} = \mathcal{L}_0 + \mathcal{V}$, so $\hat{\mathcal{I}}_e$ in equation 3 is nonlinear on

$\mathcal{V}$. This means the extended images based on the definitions in equations 1–3 properly account for the effects of multiple scattering.

It is important to note that the scattering potential $\mathcal{V}$ can be defined arbitrarily. The most common definition in migration/imaging literature (e.g., Oristaglio, 1989; Weglein et al., 2003; Symes, 2009) is that $c = c_0 + \delta c$ is comprised of a smooth background c_0 and sharp discontinuities δc (i.e., the singular part of the model). Under this definition, $\mathcal{V}$ becomes an operator that accounts for the singularities in the scattered wavefields G_S. We use this definition but point out that $\mathcal{V}$ can be defined in other ways, e.g., as a smooth time-lapse change or by incorporating attenuation (e.g., Vasconcelos et al., 2009b).

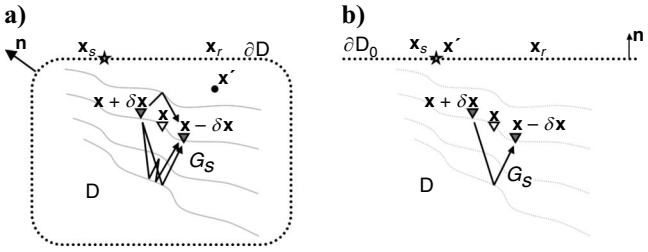

Figure 1. Geometries for two-way extended imaging using scattering reciprocity. The point $\mathbf{x}$ (white triangle) is an image point in the subsurface/model domain $\mathbb{D}$. The points $\mathbf{x} + \delta\mathbf{x}$ and $\mathbf{x} - \delta\mathbf{x}$ (gray triangles) are, respectively, the locations of pseudosources and pseudoreceivers in $\mathbb{D}$ that are displaced from $\mathbf{x}$ by a space lag $\delta\mathbf{x}$. The values $\mathbf{x}_s$ and $\mathbf{x}_r$ represent, respectively, the locations of the physical sources (stars) and receivers (black dots) used in the data acquisition. For each shot in $\mathbf{x}_s$, there are receivers $\mathbf{x}_r$ everywhere on $\partial\mathbb{D}$ or $\partial\mathbb{D}_0$; the sources themselves cover the same surfaces. The arrows represent the scattered-wave response G_S. The curved gray lines represent heterogeneity in the subsurface model (e.g., layering). (a) The most general case where the surface $\partial\mathbb{D}$ encloses the subsurface domain and the imaging-condition integration is conducted over $\mathbf{x}'$ in the volume $\mathbb{D}$ as well as on the surface. The subsurface model may contain sharp boundaries, indicated by the solid gray lines. (b) The more conventional configuration for single-scattering, Born-based imaging where integration is typically conducted over $\mathbf{x}'$ on the open surface $\partial\mathbb{D}_0$ and where sharp model discontinuities are absent (indicated by the dashed gray lines).

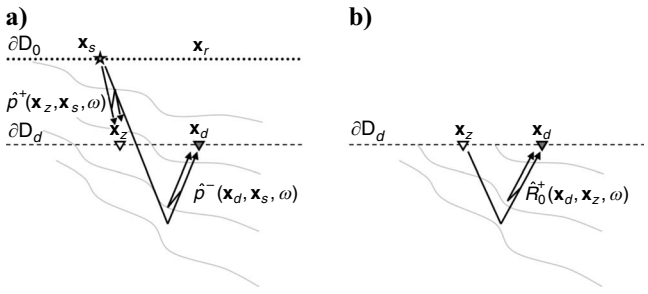

Figure 2. Geometries for one-way extended imaging using scattering reciprocity. As in Figure 1, $\mathbf{x}_s$ and $\mathbf{x}_r$ represent sources and receivers that cover the top acquisition surface $\partial\mathbb{D}_0$. The values $\mathbf{x}_z$ and $\mathbf{x}_d$ (depicted by triangles) are two arbitrary subsurface points that lie on the depth-domain surface $\partial\mathbb{D}_d$. (a) The value $\hat{p}^{\pm}$ represents full up- and downgoing fields from a source at $\mathbf{x}_s$ on $\partial\mathbb{D}_0$, depth extrapolated to $\partial\mathbb{D}_d$ from the data recorded by the receivers at all $\mathbf{x}_r \in \partial\mathbb{D}_0$ (black dots), including all multiple arrival types. (b) The upgoing reflection impulse response $\hat{R}_0^+$ (equations 4 and 5) for a pseudosource and a pseudoreceiver on the depth-domain surface $\partial\mathbb{D}_d$, which contains all upgoing primaries and multiples.

One-way extended images

In the context of one-way wave propagation (e.g., Claerbout, 1971; Fishman and McCoy, 1984; Fishman et al., 1987; Wapenaar et al., 2001; de Hoop et al., 2003), an extended image can be defined as

$$I_e(\mathbf{x},\delta\mathbf{x},\tau) = R_0^+(\mathbf{x} + \delta\mathbf{x},\mathbf{x},\tau), \tag{4}$$

where $R_0^+(\mathbf{x} + \delta\mathbf{x},\mathbf{x},\tau)$ is the finite-time upgoing reflectivity response to a downgoing field p^+ (Wapenaar et al., 2004; Wapenaar et al., 2008) for pseudosources at $\mathbf{x}$ and pseudoreceivers at $\mathbf{x} + \delta\mathbf{x}$ within the subsurface (see Figure 2). The subscript zero indicates that the response $\hat{R}_0^+$ corresponds to that of a medium that is heterogeneous below some depth level $\partial\mathbb{D}_d$ but homogeneous above it. Similar to the definition of two-way extended images in terms of G_S in equation 2, the image I_e is also a space- and time-dependent, wavefield-like object. As with the two-way case, equation 4 is a straightforward extension of the classical definition of a subsurface image as a zero-offset and zero-time reflectivity response (e.g., Claerbout, 1971), i.e., $I(\mathbf{x}) = R_0^+(\mathbf{x},\mathbf{x},\tau = 0)$.

Despite similarities in their definitions, the one-way extended image defined by equation 4 is fundamentally different from the two-way image defined in equation 2. The first and most important difference lies in the meaning of these definitions. While it follows from the definition of the two-way EI in equation 2 that $\mathcal{I}_e$ satisfies the PDE in equation 3, the one-way I_e in equation 4 is the kernel operator of the integral equation (e.g., Wapenaar et al., 2004; Wapenaar et al., 2008):

$$\hat{p}^-(\mathbf{x}_d,\mathbf{x}_s,\omega) = \int_{\mathbf{x}_z \in \partial\mathbb{D}_d} \hat{R}_0^+(\mathbf{x}_d,\mathbf{x}_z,\omega)\hat{p}^+(\mathbf{x}_z,\mathbf{x}_s,\omega)d^2\mathbf{x}_z, \tag{5}$$

where $\{\mathbf{x}_d,\mathbf{x}_z\}$ are points in the subsurface plane $\partial\mathbb{D}_d$ and where $\hat{p}^-(\mathbf{x}_d,\mathbf{x}_s,\omega)$ and $\hat{p}^+(\mathbf{x}_z,\mathbf{x}_s,\omega)$ are, respectively, up- and downgoing fields recorded at depth as a result of sources at $\mathbf{x}_s$ on the surface plane $\partial\mathbb{D}_0$. This is illustrated in Figure 2. The EI in equation 4 is obtained from $\hat{R}_0^+(\mathbf{x}_d,\mathbf{x}_z,\omega)$ by choosing $\mathbf{x}_z = \mathbf{x}$ and $\mathbf{x}_d = \mathbf{x} + \delta\mathbf{x}$ and after an inverse Fourier transform $\omega \mapsto \tau$. Therefore, although the two-way EI $\mathcal{I}_e$ in equation 2 is a scattered wavefield with physical dimensions (e.g., dimensions of pressure), its one-way counterpart I_e in equation 4 is a dimensionless operator. Furthermore, the decomposition that yields the up/down-separated fields $p^{+,-}$ imposes limitations on spatial aperture[1] (e.g., leading to a decrease in accuracy toward horizontal directions) and ignores the effects of laterally propagating or evanescent wave modes (e.g., Fishman and McCoy, 1984; Wapenaar et al., 2001). These restrictions do not apply to the two-way extended images described by equation 3.

The one-way EI we present here describes only upgoing, backscattered responses between subsurface points, whereas the two-way EI defined in terms of G_S ideally retrieves forward- and backscattered waves with no directional restrictions. Therefore, although one-way EIs retrieve only upward-propagating reflection responses, two-way EIs ideally can reconstruct transmission and reflection responses between subsurface points. In principle, the one-way EI de-

[1]One-way fields can be treated as the product of filtering two-way fields with spatially varying local wavenumber filters; see Shubin (1987) for a detailed description of the spectral properties of one-way wave propagators.

scription can be adapted to include downgoing reflections via the downgoing reflectivity operator (e.g., Wapenaar et al., 2004). This modification would, however, substantially increase the complexity of one-way imaging and is beyond the scope of this paper.

EXTENDED IMAGES FROM SCATTERING RECIPROCITY

Two-way imaging conditions

After defining the two-way EIs according to equations 1 and 2, the next step is to formally define imaging conditions that retrieve images that comply with those definitions. Because our definitions rely on retrieving the scattered fields G_S, we can use integral scattering representations to obtain the desired images (e.g., Thorbecke and Wapenaar, 2007; Wapenaar, 2007; Vasconcelos, 2008; Vasconcelos et al., 2009a; Halliday and Curtis, 2010). These scattering representations are similar to those in seismic interferometry applications (e.g., Bakulin and Calvert, 2006; Wapenaar, 2007; Vasconcelos and Snieder, 2008).

The extended images $\mathcal{I}_e$ that follow from equation 2 can be obtained reconstructing the scattered field G_S for finite times and by allowing the source and receiver locations to be arbitrarily different (see discussion about equation 2). Assuming a common $\mathbf{x}$, we write the pseudosource and receiver locations as $\mathbf{x}+\delta\mathbf{x}$ and $\mathbf{x}-\delta\mathbf{x}$, respectively (Figure 1). Using the correlation scattering representation for G_S from Vasconcelos et al. (2009b) in equation 2 then gives (Vasconcelos et al., 2009a)

$$\begin{aligned}\mathcal{I}_e(\mathbf{x},\delta\mathbf{x},\tau) &= G_S(\mathbf{x}-\delta\mathbf{x},\mathbf{x}+\delta\mathbf{x},t=\tau)\\ &= \int\left(\oint_{\partial\mathbb{D}}\frac{F(\omega)}{i\omega\rho}[\nabla p_S(\mathbf{x}-\delta\mathbf{x},\mathbf{x}',\omega)\right.\\ &\quad\left.\times p_0^*(\mathbf{x}+\delta\mathbf{x},\mathbf{x}',\omega)]\cdot\mathbf{n}d^2\mathbf{x}'\right)e^{i\omega\tau}d\omega\\ &\quad-\int\left(\oint_{\partial\mathbb{D}}\frac{F(\omega)}{i\omega\rho}[p_S(\mathbf{x}-\delta\mathbf{x},\mathbf{x}',\omega)\right.\\ &\quad\left.\times\nabla p_0^*(\mathbf{x}+\delta\mathbf{x},\mathbf{x}',\omega)]\cdot\mathbf{n}d^2\mathbf{x}'\right)e^{i\omega\tau}d\omega\\ &\quad+\int\left(\int_{\mathbb{D}}\frac{F(\omega)}{i\omega\rho}p(\mathbf{x}-\delta\mathbf{x},\mathbf{x}',\omega)\mathcal{V}(\mathbf{x}')\right.\\ &\quad\left.\times p_0^*(\mathbf{x}+\delta\mathbf{x},\mathbf{x}',\omega)d^3\mathbf{x}'\right)e^{i\omega\tau}d\omega,\end{aligned}\tag{6}$$

where ρ is density, p_0 is a reference pressure field, p_S are scattered pressure waves, and $p=p_0+p_S$. The value $F(\omega)$ is a deconvolution filter that turns the pressure fields p into impulse responses G.

Here, gradients are evaluated at the points $\mathbf{x}'$. The pressure fields in the integrand require sources at $\mathbf{x}'$ to be everywhere on the surface $\partial\mathbb{D}$ as well as in the volume $\mathbb{D}$ (Figure 1a). Also, the observation points $\mathbf{x}$ and $\mathbf{x}\pm\delta\mathbf{x}$ are inside the model and do not correspond to physical recording locations. In practice, we physically excite waves at $\mathbf{x}_s$ and record them at $\mathbf{x}_r$ on the boundary (Figure 1), so the wavefields in the integrands of equation 6 are obtained after wavefield extrapolation. Halliday and Curtis (2010) use equation 6 to arrive at a generalized formula for the scattered field for imaging where the p_S fields in the integrand are themselves replaced by another set of integrals in the context of the source-receiver interferometry formulation (Curtis and Halliday, 2010).

Once $\mathcal{I}_e$ is defined by equation 6, it is straightforward to obtain the conventional image $\mathcal{I}$ (equation 1) by setting constant $\delta\mathbf{x}=\mathbf{0}$ and $\tau=0$, which yields

$$\begin{aligned}\mathcal{I}(\mathbf{x}) &= G_S(\mathbf{x},\mathbf{x},\tau=0)\\ &= \int\left(\oint_{\partial\mathbb{D}}\frac{F(\omega)}{i\omega\rho}[\nabla p_S(\mathbf{x},\mathbf{x}',\omega)p_0^*(\mathbf{x},\mathbf{x}',\omega)]\cdot\mathbf{n}d^2\mathbf{x}'\right)d\omega\\ &\quad-\int\left(\oint_{\partial\mathbb{D}}\frac{F(\omega)}{i\omega\rho}[p_S(\mathbf{x},\mathbf{x}',\omega)\nabla p_0^*(\mathbf{x},\mathbf{x}',\omega)]\cdot\mathbf{n}d^2\mathbf{x}'\right)d\omega\\ &\quad+\int\left(\int_{\mathbb{D}}\frac{F(\omega)}{i\omega\rho}p(\mathbf{x},\mathbf{x}',\omega)\mathcal{V}(\mathbf{x}')p_0^*(\mathbf{x},\mathbf{x}',\omega)d^3\mathbf{x}'\right)d\omega.\end{aligned}\tag{7}$$

Although we refer to this equation as a conventional image, typical implementations of two-way imaging by, e.g., reverse-time migration do not use formulation 7.

The gradient terms in the integrands of equation 6 imply a requirement for acquiring data with monopole and dipole sources and receivers (e.g., Fokkema and van den Berg, 1993; Wapenaar and Fokkema, 2006). Dipole (i.e., particle velocity) sources and receivers are seldom available in real-life seismic surveys, so it is convenient to use the far-field approximation $\nabla p\cdot\mathbf{n}=i\omega c^{-1}p$ (e.g., Wapenaar and Fokkema, 2006) to recast equation 6 as

$$\begin{aligned}\mathcal{I}_e(\mathbf{x},\delta\mathbf{x},\tau) &= \int\left(\oint_{\partial\mathbb{D}}\frac{2F(\omega)}{\rho c}p_S(\mathbf{x}-\delta\mathbf{x},\mathbf{x}',\omega)\right.\\ &\quad\left.\times p_0^*(\mathbf{x}+\delta\mathbf{x},\mathbf{x}',\omega)d^2\mathbf{x}'\right)e^{i\omega\tau}d\omega\\ &\quad+\int\left(\int_{\mathbb{D}}\frac{F(\omega)}{i\omega\rho}p(\mathbf{x}-\delta\mathbf{x},\mathbf{x}',\omega)\mathcal{V}(\mathbf{x}')\right.\\ &\quad\left.\times p_0^*(\mathbf{x}+\delta\mathbf{x},\mathbf{x}',\omega)d^3\mathbf{x}'\right)e^{i\omega\tau}d\omega.\end{aligned}\tag{8}$$

This far-field radiation condition can introduce errors that distort the retrieved $\mathcal{I}_e$. These errors arise in the form of dynamic effects together with possible artifact arrivals, depending on the model and acquisition geometry. We point the reader to Wapenaar and Fokkema (2006), Vasconcelos et al. (2009b), and Ramírez and Weglein (2009) for further discussions on the effects of the far-field radiation condition.

In the context of imaging conditions, the pressure fields in the integrands of equations 6 and 8 are obtained from wavefield extrapolation and not from direct physical experiments. When the fields in question are in fact direct measurements, then equations 6 and 8 are the same as used for seismic interferometry applications (e.g., Bakulin and Calvert, 2006; Vasconcelos et al., 2009b). The volume integral in equations 6 and 8 accounts for dynamic and kinematic effects associated with forward scattering (i.e., transmission effects) and multiple scattering, i.e., nonlinear interactions of the fields p_0 and p_S

with the potential $\mathcal{V}$. Although its precise contributions are model dependent, the general behavior of this volume term is similar to that of the classical Lippmann-Schwinger scattering integral but under the action of time-advanced field p_0^* instead of the usual time-retarded field p_0. A more in-depth discussion is presented in Vasconcelos et al. (2009b).

In many of the interferometry applications (e.g., Bakulin and Calvert, 2006), the volume terms of equations 6 and 8 can be ignored (Vasconcelos et al., 2009b). For general imaging applications, however, the volume integrals cannot be ignored (Vasconcelos, 2008; Vasconcelos et al., 2009a; Halliday and Curtis, 2010). The connection between calculating extended images and seismic interferometry arises directly from the image definitions in equations 1 and 2 together with the use of scattering reciprocity integrals (e.g., Wapenaar, 2007; Vasconcelos, 2008; Vasconcelos et al., 2009a; Halliday and Curtis, 2010). A similar analogy exists for the one-way formulation as well.

One-way imaging conditions

Given that the depth-domain fields $\hat{p}^-(\mathbf{x}_d,\mathbf{x}_s,\omega)$ and $\hat{p}^+(\mathbf{x}_z,\mathbf{x}_s,\omega)$ (equation 5 and Figure 2) can be generated from the acquired data via wavefield extrapolation, extended images as defined in equation 4 can obtained by solving equation 5 for $\hat{R}_0^+$. The integral representation in equation 5 also can be expressed in discrete matrix-operator form, i.e., $\hat{\mathbf{P}}^- = \hat{\mathbf{R}}_0^+\hat{\mathbf{P}}^+$ (Berkhout, 1982). Here, the columns of the fixed-frequency matrices $\hat{\mathbf{P}}^\pm$ correspond to $\hat{p}^\pm(\mathbf{x},\mathbf{x}_i,\omega)$ for a fixed source location $\mathbf{x}_i$ and variable receiver location $\mathbf{x}$, whereas the rows represent $\hat{p}^-(\mathbf{x}_j,\mathbf{x},\omega)$ for a fixed receiver location $\mathbf{x}_j$ and variable source location $\mathbf{x}$ at a particular fixed depth level. Figure 3 illustrates the operator $\hat{R}_0^+(\mathbf{x}_d,\mathbf{x}_z,\omega)$ as a discrete matrix $\hat{\mathbf{R}}_0^+$ for a fixed chosen frequency. De Bruin et al. (1990) rely on $\hat{\mathbf{R}}_0^+$ in the context of linear inversion of primary reflections as a function of subsurface scattering angle.

A pseudoinverse reflectivity operator $\bar{\mathbf{R}}_0^+$ can then be obtained from, say, a regularized least-squares inversion as (e.g., Hansen, 1997; Wapenaar et al., 2008)

$$\bar{\mathbf{R}}_0^+ = \mathbf{P}^-(\mathbf{P}^+)^\dagger[\mathbf{P}^+(\mathbf{P}^+)^\dagger + \epsilon^2\mathbf{\Lambda}]^{-1}, \qquad (9)$$

where the dagger (†) stands for the conjugate transpose, $\mathbf{\Lambda}$ is a shaping/regularization operator, and ε is a weighting factor. With appropriate choices for ε and $\mathbf{\Lambda}$, equation 9 can yield an acceptable estimate of the reflectivity operator, i.e., $\bar{\mathbf{R}}_0^+ \approx \hat{\mathbf{R}}_0^+$.

To then obtain an extended image I_e (e.g., equation 4) from the reflectivity operator, one can select an appropriate subset of $\hat{\mathbf{R}}_0^+$. For example, selecting a column of the $\hat{\mathbf{R}}_0^+$ (blue outline in Figure 3) operator (Figure 3) and choosing a fixed $\mathbf{x}_z = \mathbf{x}$ for variable $\mathbf{x}_d = \mathbf{x} + \delta\mathbf{x}$ yields precisely the extended image defined by equation 4. This choice leads to an extended image of a common-source geometry, similar to that discussed for the two-way case of equation 2. Conversely, extracting the rows of $\hat{\mathbf{R}}_0^+$ (green outline in Figure 3) yields extended images with a common-receiver pseudoacquisition geometry. Another choice would be to extract the antidiagonal elements of $\hat{\mathbf{R}}_0^+$ (red outline in Figure 3) by setting $\mathbf{x}_d = \mathbf{x} - \delta\mathbf{x}$ and $\mathbf{x}_z = \mathbf{x} + \delta\mathbf{x}$ for a fixed image point $\mathbf{x}$; this would then yield $I_e(\mathbf{x},\delta\mathbf{x},\tau) = R_0^+(\mathbf{x} - \delta\mathbf{x},\mathbf{x} + \delta\mathbf{x},\tau)$, i.e., an extended image with a common-midpoint geometry. This geometry would be the same as that of the two-way $\mathcal{I}_e$ described by equations 6 and 8 and illustrated in Figure 1. Although these different EI geometries can be extracted from different combinations of the elements of the $\hat{\mathbf{R}}_0^+$-matrix, $\hat{\mathbf{R}}_0^+$ itself provides the most general description of the possible pseudoacquistion geometries for the EIs.

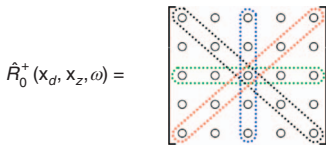

Figure 3. The operator $\hat{\mathbf{R}}_0^+$, representing $\hat{R}_0^+(\mathbf{x}_d,\mathbf{x}_z,\omega)$ in discrete matrix form at a chosen $\partial\mathbb{D}_d$ (Figure 2b) and for a fixed frequency ω. Each row of the matrix corresponds to a discrete pseudoreceiver location $\mathbf{x}_d$ and variable $\mathbf{x}_z$, whereas columns represent a fixed pseudosource coordinate $\mathbf{x}_z$ and variable $\mathbf{x}_d$. The dotted contours highlight different choices of geometries of one-way extended images.

As with the two-way imaging conditions presented above, extended imaging based on the one-way reciprocity theorem in equation 5 is directly related to the practice of seismic interferometry. Wapenaar et al. (2008) present the method of interferometry by multidimensional deconvolution (MDD) that relies on equations 5 and 9 to estimate $\hat{\mathbf{R}}_0^+$ from observed up- and downgoing fields. Our approach is the same as that of Wapenaar et al. (2008) except that the fields used to estimate the reflectivity operator are depth-extrapolated fields as opposed to physically observed data as used in interferometry (Figure 2).

WAVEFIELD EXTRAPOLATION FOR NONLINEAR EXTENDED IMAGES

Two-way extrapolation

Although interferometry relies on observed fields p_0 and p_S (e.g., Bakulin and Calvert, 2006; Vasconcelos, 2008), in two-way wave-equation imaging (equation 8) these fields result from extrapolating (i.e., redatuming) the fields recorded at the acquisition surface to the image point $\mathbf{x}$ (e.g., Claerbout, 1985; Sava and Vasconcelos, 2010). In imaging, $p_0(\mathbf{x},\mathbf{x}',\omega)$ (e.g., equation 8) are depth-extrapolated source wavefields, which translates to numerically solving this initial-value problem:

$$\begin{cases} \hat{\mathcal{L}}_0\hat{p}_0 = 0, \quad \hat{p}_0 = \hat{p}_0(\mathbf{x},\mathbf{x}',\omega), \mathbf{x} \in \mathbb{D} \text{ and } \mathbf{x}' \in \mathbb{D}\cup\partial\mathbb{D}, \text{with} \\ p_0(\mathbf{x},\mathbf{x}_s,t) = s(t) * \delta(\mathbf{x} - \mathbf{x}_s)\delta(t) \quad \text{as ICs, for all } \mathbf{x}_s \in \partial\mathbb{D}; \end{cases} \qquad (10)$$

where IC stands for initial conditions, $\mathbf{x}_s$ are the acquisition source coordinates (Figure 1a), δ is the Dirac delta, $s(t)$ is the time-domain source signature, and the asterisk ($*$) stands for convolution.

The problem in equation 10 is translated as forward modeling each shot at $\mathbf{x}' = \mathbf{x}_s \in \partial\mathbb{D}$ to every point $\mathbf{x}$ inside $\mathbb{D}$ (Figure 1a). In addition, based on the fields from surface sources recorded at every $\mathbf{x} \in \mathbb{D}$, the response from each $\mathbf{x}'$ inside $\mathbb{D}$ to every $\mathbf{x} \in \mathbb{D}$ must also be calculated. This latter step can be performed, for example, with the method of van Manen et al. (2005). Solving the initial-value problem described by equation 10 results in the $\hat{p}_0(\mathbf{x},\mathbf{x}',\omega)$ fields required by the extended imaging condition in equation 8. This reference field p_0 is traditionally called the source wavefield in migration practice. The source-wavefield calculation in equation 10 is analogous to that performed in current migration practice, with the additional step of

modeling the response of sources that are also inside the subsurface. This additional step is necessary for evaluating the volume integral in equation 8.

The next step is to compute the scattered fields $\hat{p}_S(\mathbf{x},\mathbf{x}',\omega)$, or the receiver wavefields, necessary for evaluating the integrands in equation 8. These are obtained by solving the boundary-value problem:

$$\begin{cases} \hat{\mathcal{L}}\hat{p}_S = -\mathcal{V}\hat{p}_0, \quad \hat{p}_S = \hat{p}_S(\mathbf{x},\mathbf{x}',\omega), \mathbf{x} \in \mathbb{D} \text{ and } \mathbf{x}' \in \mathbb{D} \cup \partial\mathbb{D}, \text{with} \\ \hat{p}_S(\mathbf{x}_r,\mathbf{x}_s,\omega) = \hat{d}_S^*(\mathbf{x}_r,\mathbf{x}_s,\omega) \quad \text{as BC for all } \mathbf{x}_{s,r} \in \partial\mathbb{D} \end{cases}, \tag{11}$$

where BC stands for boundary conditions, which consist of $\hat{d}_S^*(\mathbf{x}_r,\mathbf{x}_s,\omega)$, the full, time-reversed scattered wavefield from the acquired common-shot data. The values $\mathbf{x}_r$ are the acquisition receiver coordinates (Figure 1a). Note that the scattered-wave data $\hat{d}_S^*(\mathbf{x}_r,\mathbf{x}_s,\omega)$ consist of the full recorded data minus the waves that propagate in the reference model (e.g., the direct arrivals). This, together with the use of the scattering PDE in equation 11 ensures that there are no background waves propagated in the receiver wavefields.

Under this formulation, all nonlinear effects in two-way imaging are restricted to the receiver wavefields only because equation 11 operates with the scattering potential $\mathcal{V}$ whereas the source fields described by equation 10 are functions of the smooth background model. In addition to boundary conditions for the pressure scattered field, the ideal back propagation of recorded scattered fields also requires appropriate boundary conditions on the gradient of pressure or, alternatively, on particle velocity fields. These can be additional field records of vectorial acoustic fields or can be inferred from pressure data with additional assumptions. We leave these specific back-propagation issues to future studies.

It is important to note that the receiver extrapolation approach in equation 11 differs from usual migration practice in three points. First, the boundary value problem described in equation 11 solves the inhomogeneous PDE for scattered fields (e.g., equation 3) as opposed to a homogeneous wave equation (e.g., similar to that in equation 10). Consequently, the source wavefield p_0 that results from solving the problem in equation 10 must in fact be used for extrapolating the receiver or scattered wavefield p_S as described by the problem in equation 11.

Second, receiver wavefield extrapolation according to equation 11 uses the operators $\mathcal{L}$ and $\mathcal{V}$, which differ from the smooth operator $\mathcal{L}_0$ for the source wavefield (equation 10). In other words, the models for source and receiver extrapolation are different. This allows for modeling multiples when extrapolating the receiver wavefields because the wavefields $\hat{p}_0$ and $\hat{p}_S$ are allowed to interact with the singularities in $\mathcal{L}$ and $\mathcal{V}$ (equation 11).

Third, as with the source wavefield calculation above, the field $\hat{p}_S(\mathbf{x},\mathbf{x}',\omega)$ must be computed for $\mathbf{x}' \in \mathbb{D}$ in additional to surface sources only (i.e., $\mathbf{x}' = \mathbf{x}_s \in \partial\mathbb{D}$). In the formulation by Halliday and Curtis (2010), the extrapolation for the receiver wavefield p_S is analitically expressed in terms of scattering representation integrals (Vasconcelos et al., 2009b) and inserted into equation 6, as opposed to the boundary value problem approach we present here.

One-way extrapolation

Wavefield extrapolation for generating one-way extended images is similar to current practice in one-way migration. The depth-domain source wavefield $\mathbf{P}^+ = \hat{p}^+(\mathbf{x}_z,\mathbf{x}_s,\omega)$ (equations 5 and 9) is generated via

$$\begin{cases} \mathbf{P}^+ = \mathbf{T}^+\mathbf{S}_0^+ & \text{with} \\ \mathbf{S}_0^+ = \delta(\mathbf{x}-\mathbf{x}_s)s(\omega) & \text{for all } \mathbf{x}_s \in \partial\mathbb{D}_0 \end{cases}, \tag{12}$$

where $\mathbf{S}_0^+$ is the discrete version of $\hat{s}_0^+(\mathbf{x}=\mathbf{x}_r,\mathbf{x}_s,\omega)$, which are the source data at the acquisition surface (Figure 2); $s(\omega)$ is the frequency-domain source excitation function; and $\mathbf{T}^+$ is a modeling operator for downgoing transmission that maps surface data at $\mathbf{x}_r \in \partial\mathbb{D}_0$ to subsurface-domain wavefields at $\mathbf{x}_z \in \partial\mathbb{D}_d$ (Figure 2). In parallel with the source-wavefield calculation in equation 12, the one-way receiver fields $\mathbf{P}^- = \hat{p}^-(\mathbf{x}_d,\mathbf{x}_s,\omega)$ (equations 5 and 9; Figure 2) are obtained from

$$\begin{cases} \mathbf{P}^- = (\mathbf{T}^-)^{-1}\mathbf{D}_0^- & \text{with} \\ \mathbf{D}_0^- = \hat{d}_0^-(\mathbf{x}_r,\mathbf{x}_s,\omega) & \text{for all } \{\mathbf{x}_s,\mathbf{x}_r\} \in \partial\mathbb{D}_0 \end{cases}, \tag{13}$$

where $\mathbf{D}_0^- = \hat{d}_0^-(\mathbf{x}_r,\mathbf{x}_s,\omega)$ are the full, upgoing reflection data acquired for all shots and receivers on the acquisition surface. The value $\mathbf{T}^-$ is the modeling operator for upgoing transmission that datums depth-domain fields at all $\mathbf{x}_d \in \partial\mathbb{D}_d$ to surface data at $\mathbf{x}_r \in \partial\mathbb{D}_0$ (Figure 2). Under flux-normalized up/downgoing wavefield decomposition, $\mathbf{T}^-$ is the transpose of $\mathbf{T}^+$ (equation 12). The inverse of $\mathbf{T}^-$ thus maps the reflection data at the surface to the receiver wavefield in the subsurface.

There are three main distinctions between the wavefield-extrapolation steps described by equations 12 and 13 and those in current one-way migration approaches. First, the upgoing surface data $\mathbf{D}_0^- = \hat{d}_0^-(\mathbf{x}_r,\mathbf{x}_s,\omega)$ contain the full recorded reflection response (i.e., with all upgoing multiples), as opposed to only primary reflection data. Second, the modeling operators $\mathbf{T}^\pm$ are meant to be full transmission response operators (e.g., Thorbecke, 1997; Wapenaar et al., 2004; Mulder, 2005), i.e., they model amplitude-preserving transmitted fields that contain direct arrivals as well as transmission multiples. Malcolm et al. (2009) offer a scattering-series approach that can be used for practical implementation of the nonlinear $\mathbf{T}^\pm$ operators.

Finally, we note that the inverse operator $(\mathbf{T}^-)^{-1}$ is used to back-propagate the receiver data $\mathbf{D}_0^-$, whereas common practice does not rely on inverse transmission operators. In principle, these three differences combined allow for proper modeling of multiples in the depth-extrapolated fields, which is a key element necessary for inversion of the full nonlinear reflectivity operator in equations 5 and 9. In the next section, we address differences between the steps above and the computation of extended images in current migration practice.

EXTENDED IMAGES IN CURRENT MIGRATION PRACTICE

Unlike nonlinear imaging conditions and wavefield extrapolation that models multiples in the depth-extrapolated fields, most current migration practices rely on the Born approximation (e.g., Claerbout, 1971; Stolt and Weglein, 1985) for one- and two-way imaging. The objective behind most migration schemes is structural characterization, so it is not uncommon that additional approximations ignore amplitude-related effects in extrapolation and imaging. As a consequence, these approximations bring two major simplifications for practically implementing EIs: (1) all of the wavefield extrapolation can be carried out with a single, smooth wavespeed model and (2) evaluation of the imaging conditions is substantially simpler and becomes effectively the same for one- and two-way imaging.

Two-way imaging in current migration practice is typically achieved by adapting the receiver wavefield extrapolation in equation 11 to

$$\begin{cases} \hat{\mathcal{L}}_0\hat{p}_S = 0 \quad \text{for } \hat{p}_S(\mathbf{x},\mathbf{x}',\omega) \text{ with } \mathbf{x}\in\mathbb{D},\mathbf{x}'=\mathbf{x}_s\in\partial\mathbb{D}_0 \\ \hat{p}_S(\mathbf{x}_r,\mathbf{x}_s,\omega) = \hat{d}_P^*(\mathbf{x}_r,\mathbf{x}_s,\omega) \quad \text{for all } \mathbf{x}_{s,r}\in\partial\mathbb{D}_0 \end{cases}, \tag{14}$$

where the primary-only data $\hat{d}_P(\mathbf{x}_r,\mathbf{x}_s,\omega)$ replace the full recorded scattered waves $\hat{d}_S(\mathbf{x}_r,\mathbf{x}_s,\omega)$ in equation 11. These data are back-extrapolated with the smooth operator $\mathcal{L}_0$, just as used for the source wavefield extrapolation described by equation 10. The homogeneous PDE $\hat{\mathcal{L}}_0\hat{p}_S=0$ is not equivalent to the Born approximation of the inhomogeneous PDE in equation 11. Proper Born modeling would require including the forcing term $-\mathcal{V}_{\text{Born}}\hat{p}_0$, i.e., solving for $\hat{\mathcal{L}}_0\hat{p}_S=-\mathcal{V}_{\text{Born}}\hat{p}_0$ instead (here, $\mathcal{V}_{\text{Born}}$ represents $\mathcal{V}$ after linearization on the singular part of the model, e.g., δc). Sources and receivers are no longer assumed to enclose the medium and are instead available only over a finite surface $\partial\mathbb{D}_0$ (Figure 1b). Although this assumption mimics realistic geophysical data where physical sources and receivers are only available at the earth's surface, it also typically introduces artifacts in the wavefield reconstruction and interferometry processes (e.g., Wapenaar, 2006; Wapenaar and Fokkema, 2006). Note that the responses of source and receiver wavefields, i.e., $\hat{p}_{0,S}(\mathbf{x},\mathbf{x}',\omega)$, are computed only for points $\mathbf{x}'=\mathbf{x}_s$ on the surface. The fields extrapolated in equations 10 and 11 need additional extrapolated sources at the points $\mathbf{x}'$ inside the subsurface volume.

By extrapolating the receiver wavefield according to equation 14 as opposed to equation 11, the nonlinear interactions between the back-propagating receiver wavefield and the model discontinuities present in the operators $\mathcal{L}$ and $\mathcal{V}$ are ignored. When ignoring the contributions of model discontinuities in the extrapolation step (i.e., by ignoring the Born forcing term $\mathcal{V}\hat{p}_0$), current two-way migration algorithms also ignore the volume integral in the imaging condition in equation 8. Thus, an EI can be approximated from equation 8 as the surface integral:

$$\mathcal{I}_e(\mathbf{x},\delta\mathbf{x},\tau)\approx\int\left(\int_{\partial\mathbb{D}_0}\frac{2F(\omega)}{\rho c}p_S(\mathbf{x}-\delta\mathbf{x},\mathbf{x}_s,\omega)\times p_0^*(\mathbf{x}+\delta\mathbf{x},\mathbf{x}_s,\omega)d^2\mathbf{x}_s\right)e^{i\omega\tau}d\omega, \tag{15}$$

where $\partial\mathbb{D}_0$ is a subset of $\partial\mathbb{D}$ (Figure 1) and $\mathbf{x}'=\mathbf{x}_s$ as shown in equation 14. This result yields an estimate for an EI that is a straightforward extension of the conventional correlation-based imaging condition, obtained by adding space lags $\delta\mathbf{x}$ and time lags τ to the cross-correlation of source wavefields p_0 and receiver wavefields p_S (Sava and Vasconcelos, 2010).

An analogous approach is taken to generate one-way EIs under the single-scattering approximation, using a smooth wavespeed model. For one-way imaging, source wavefield extrapolation is done according to equation 12, with the full transmission operator $\mathbf{T}^+$ replaced by $\mathbf{T}_0^+$, the transmission operator in a smooth medium (e.g., Thorbecke, 1997; Wapenaar et al., 2004). A similar replacement takes place in the receiver wavefield extrapolation: $\mathbf{T}^-$ is replaced by its smooth medium counterpart $\mathbf{T}_0^-$. Additionally, given the computational challenges involved with computing the inverse of the transmission operator (equation 13), $(\mathbf{T}_0^-)^{-1}$ is typically replaced by the conjugate transpose $(\mathbf{T}_0^-)^\dagger$.

Once one-way source and receiver wavefields are extrapolated using the smooth transmission operators $\mathbf{T}_0^+$ and $(\mathbf{T}_0^-)^\dagger$, the image is estimated by crosscorrelating the resulting source and receiver fields, i.e.,

$$\widetilde{\mathbf{R}}_0^+\approx\mathbf{P}^-(\mathbf{P}^+)^\dagger, \tag{16}$$

which is an approximation to the inverse in equation 9 (e.g., Claerbout, 1971; Wapenaar et al., 2008). The standard one-way migrated image is then extracted from the diagonal elements of $\widetilde{\mathbf{R}}_0^+$ (black outline in Figure 3).

From the $\widetilde{\mathbf{R}}_0^+$ matrix (equation 16), EIs can be obtained by selecting other specific combinations of elements. For example, the off-diagonal elements of $\widetilde{\mathbf{R}}_0^+$ (red outline in Figure 3) yield the extended image $I_e(\mathbf{x},\delta\mathbf{x},\tau)=\widetilde{R}_0^+(\mathbf{x}-\delta\mathbf{x},\mathbf{x}+\delta\mathbf{x},t=\tau)$, which, based on equation 16, can be directly evaluated via the integral

$$\begin{aligned} I_e(\mathbf{x},\delta\mathbf{x},\tau) &= \widetilde{R}_0^+(\mathbf{x}-\delta\mathbf{x},\mathbf{x}+\delta\mathbf{x},\tau) \\ &= \int\left(\int_{\partial\mathbb{D}_0} p^-(\mathbf{x}-\delta\mathbf{x},\mathbf{x}_s,\omega) \times\{p^+(\mathbf{x}+\delta\mathbf{x},\mathbf{x}_s,\omega)\}^* d^2\mathbf{x}_s\right)e^{i\omega\tau}d\omega. \end{aligned} \tag{17}$$

Thus, in current one-way migration practice, we can readily generate an EI by adding space and time lags to the conventional crosscorrelation of receiver and source wavefields (p^- and p^+, respectively, in equation 17), followed by a summation over sources $\mathbf{x}_s$ on the acquisition plane $\partial\mathbb{D}_0$.

Figures 4 and 5 provide a numerical example from the Sigsbee model of a one-way EI generated using equation 17. The conventional image (Figure 4b) corresponds to the diagonal elements of the estimated $\widetilde{\mathbf{R}}_0^+$ matrix (equation 16) evaluated at $\tau=0$. Because it is an approximate estimate of $\widetilde{R}_0^+(\mathbf{x},\mathbf{x},\tau=0)$, the conventional image is commonly interpreted as a representation of the structure of the true model (Figure 4a).

However, the EI in Figure 5 (with Figure 6 showing the geometry of the panels in Figure 5) shows that extended images appear similar to images of recorded data, i.e., time- and space-dependent band-limited signals with characteristic moveout signatures (in Figure 5, $\delta\mathbf{x}$ has components $\{\lambda_x,\lambda_z\}$). This is consistent with the reciprocity-based definitions of the EI as given by equations 4, 9, and 16, which show that an EI is reconstructed reflectivity data acquired by pseudo-sources and receivers in the subsurface model. This reconstruction is analogous to data reconstruction by seismic interferometry (e.g., Bakulin and Calvert, 2006; Wapenaar and Fokkema, 2006), with the distinction that the extended imaging conditions are computed with extrapolated image-domain fields as opposed to actual recordings.

Although the reflectivity response reconstructed in the EI in Figure 5 is predominantly causal as expected from the definition in equation 4, arrivals are also present for $\tau<0$ as a result of the approximation made in using only the adjoint of $\mathbf{P}^+$ and not its inverse (see equations 9 and 16). Furthermore, the proper reflectivity moveout signatures (Sava and Vasconcelos, 2010) are reconstructed only for $\tau>0$ and $\lambda_x<0$ because the towed-streamer acquisition of the Sigsbee synthetic data only allows for receivers to be placed on one side of the source locations.

DISCUSSION

We define EIs for one- and two-way imaging explicitly as scattered fields or, respectively, reflectivity operators that are excited

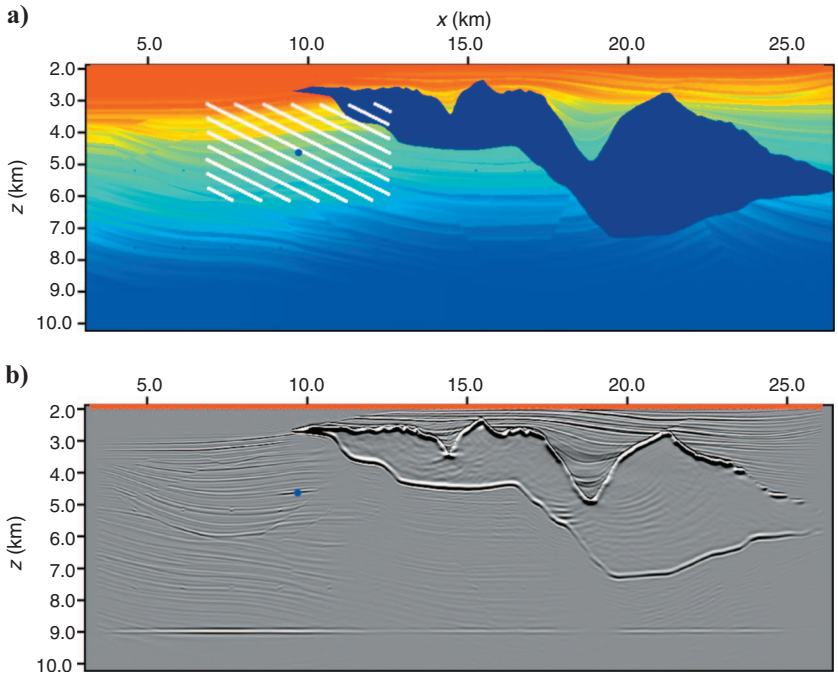

Figure 4. Sigsbee numerical example. (a) True wavespeed model. (b) Conventional one-way migrated image. The blue dot in both views shows the location $\mathbf{x}$ of the extended image portrayed in Figure 5. The red dots show the location of the surface acquisition shots $\mathbf{x}_s \in \partial\mathbb{D}_0$. Note that source coverage is dense, causing the red dots to appear as a red line at the top. The area highlighted by white lines in (a) indicates the spatial coverage of space lags $\delta\mathbf{x}$ in the extended image (Figure 5). The EI in Figure 5 is an approximate reconstruction of the scattered waves excited at $\mathbf{x}+\delta\mathbf{x}$ somewhere inside the white-highlighted area and recorded at $\mathbf{x}-\delta\mathbf{x}$. The original acquired data are laid out in a towed-streamer geometry, whereby the recording receivers lie only on the right-hand side of the shots.

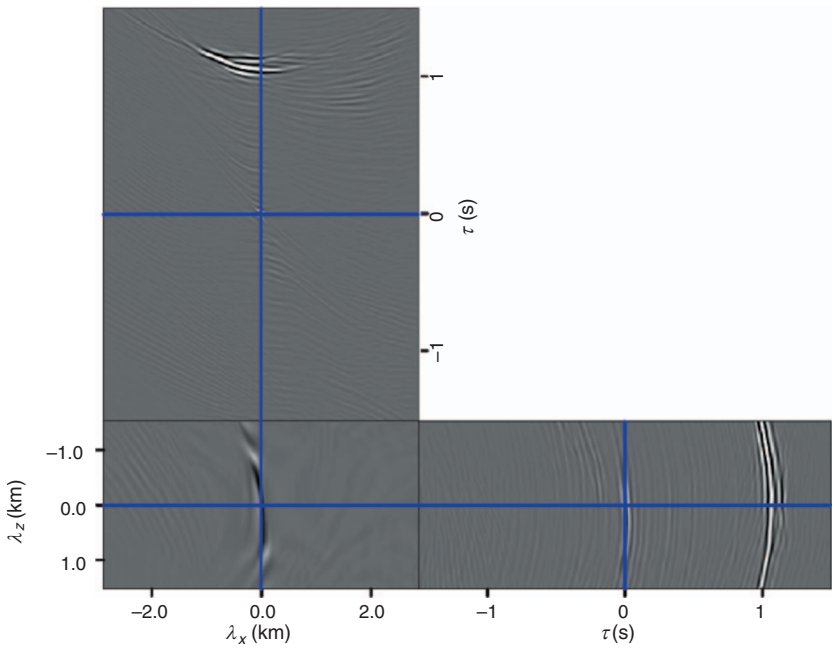

Figure 5. A one-way, full EI common-midpoint geometry, i.e., $I_e(\mathbf{x},\delta\mathbf{x},\tau)=\widetilde{R}_0^+(\mathbf{x}-\delta\mathbf{x},\mathbf{x}+\delta\mathbf{x},t=\tau)$. The EI is for a fixed $\mathbf{x}$ location (indicated by the blue dot in Figure 4) and for varying $\delta\mathbf{x}$ and τ. The space lag $\delta\mathbf{x}$ has components $\{\lambda_x,\lambda_z\}$, shown on the figure axes. The τ-axis is the time-lag variable. The planes in this figure can be interpreted as the planes intersecting at the origin of the EI cube illustrated by Figure 6. The blue lines denote the intersection of such planes.

and recorded within the subsurface and for finite times. These definitions for an image (according to equations 2 and 4), although consistent with concepts originally offered by Claerbout (e.g., 1971, 1985), differ from most formal definitions for an image, which target direct reconstruction of discontinuities in earth parameters, e.g., scattering potential $\mathcal{V}$ (e.g., Prosser, 1969; Beylkin, 1985; Stolt and Weglein, 1985; Esmersoy and Oristaglio, 1988; Weglein et al., 2003; Symes, 2008). Instead, by defining EIs in terms of space- and time-dynamic objects such as the two-way wavefield G_S or the one-way reflectivity operator R_0^+, we use wavefield reciprocity (e.g., Fokkema and van den Berg, 1993; Wapenaar et al., 2008; Vasconcelos et al., 2009b) to derive formal expressions for our nonlinear extended imaging conditions.

By invoking integral reciprocity relations and defining EIs as subsurface-domain scattering experiments, we draw an explicit connection between computing extended images via migration-based imaging by wavefield extrapolation and current practices in seismic interferometry. In fact, the integral representations we propose for generating EIs are the same as those practiced in seismic interferometry. The scattering representation we use for our two-way extended imaging condition is directly analogous to that in scattered-wave seismic interferometry as discussed by Bakulin and Calvert (2006), Vasconcelos et al. (2009b), and Wapenaar et al. (2010). Likewise, our one-way EI formulation is based on the one-way approach of Wapenaar et al. (2008).

When the imaging objective is structural characterization, it is common for current migration practice to rely on the single-scattering approximation and to ignore amplitude effects. In that case, the one- and two-way extended imaging conditions are essentially the same calculation (described by equations 14 and 17): a straightforward crosscorrelation of receiver and source-depth-domain wavefields followed by summing over all shots on the acquisition surface. The only difference is that the source and receiver wavefields are generated via one- and two-way extrapolation. This explicitly connects our formulation to common practice in migration imaging widely used today. However, this similarity between one- and two-way EIs exhibited by equations 14 and 17 occurs only because of the approximations involved. In their more general form, reciprocity-based two-way EIs are substantially different from their one-way counterparts in terms of their meaning as well as the required computations. These differences, however, should only necessarily be addressed in imaging practice if the objective is to deal with nonlinear effects in the imaging process, such as the migration of multiples or amplitude corrections resulting from transmis-

sion effects. Consistent with our findings, Halliday and Curtis (2010) show that Oristaglio's (1989) two-way inversion formula, a Born-inversion extension to Claerbout's imaging condition (1971), explicitly follows from interferometry-based integral relations.

The reciprocity-based integrals used for interferometry make no single-scattering assumptions and in principle reconstruct full nonlinear scattering responses, so our imaging conditions based on image-domain interferometry are suitable for dealing with nonlinear imaging such as multiple-scattered arrivals and associated amplitude effects. To account for nonlinear effects properly in the one- and two-way cases, current extrapolation practices must be modified such that nonlinearity is accounted for at the modeling stage. Although nonlinear transmission operators must be used for source and receiver wavefields in one-way imaging, in the two-way approach, only the receiver wavefields include nonlinear effects, and their modeling becomes dependent on previously computed source wavefields.

Apart from necessary modifications in the wavefield extrapolation step, the imaging conditions that generate nonlinear EIs also differ from standard migration practice. In the two-way case, apart from evaluating a surface integral of crosscorrelated source and receiver wavefields (akin to source stacking typically conducted in shot-profile migration), an extra volume integral term must be evaluated. Concurrent with our analysis, Halliday and Curtis (2010) show that the volume terms are necessary for nonlinear imaging as well as for imaging based on Born inversion (Oristaglio, 1989). Although there is no volume integral term to be computed in generating one-way EIs, these in turn require inversion of the full source-wavefield data matrix. At this point, computing the two-way volume integral or the one-way data matrix inverse presents unsolved computational challenges in computing nonlinear EIs practically. These issues are the subject of further investigation.

It is important to emphasize that the greatest challenge in computing nonlinear EIs in practice is, at the same time, the main justification for why we should generate them in the first place. The computation of one- and two-way EIs requires knowledge not only of the smooth migration velocity model but also of the discontinuities (i.e., the singularities) in the subsurface model. That information is obviously not available at the outset of a seismic imaging experiment. It is precisely for determining velocity models, e.g., via wave-equation, image-domain inversion approaches, that the concept of image extensions was developed. Symes (2008, and references therein) provides a comprehensive description of the role of extended images in the velocity inversion problem within the context of differential semblance optimization.

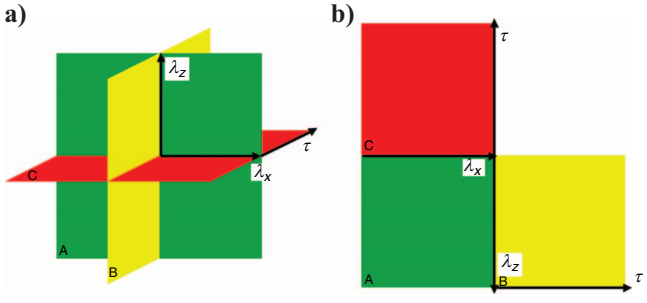

Figure 6. (a) Each point in the conventional image in Figure 4b yields an EI cube in the $\delta\mathbf{x} = (\lambda_x, \lambda_z)^T$ and τ variables. Figure 5 shows a subset of the full EI cube from the blue dot location in Figure 4b, unfolded from the planes in (a) according to the illustration in (b).

Sava and Vasconcelos (2010) show that EIs can bring additional sensitivity to the wavespeed models used in current migration practice and can help advance migration-based methods for inverting background wavespeed models. Incorporating EIs in current migration schemes is in itself potentially beneficial for increasing sensitivity to background migration wavespeed models, and our nonlinear EI formulation can be used to devise nonlinear finite-frequency inversions whose objective functions act in the subsurface image domain. Such approaches would bring the advantages of image extensions and differential semblance as advocated by Symes (2008) when designing practical numerical solutions to the nonlinear seismic inverse scattering problem (e.g., Tarantola, 1984; Rose et al., 1985; Weglein et al., 2003; Symes, 2009). Including information from multiples and nonlinear amplitude effects in EI-based inversion approaches can greatly increase model sensitivity but can also result in highly unstable inversion algorithms. The practical design of such EI-based nonlinear inverse methods remains a challenge for future research. Halliday and Curtis (2010) show that scattering-based EIs are formally connected to exact Born inverse scattering formulations and are thus suitable for extension to more sophisticated nonlinear problems.

On a more practical note, our EI formulation can contribute immediately to current migration routines. For instance, recent examples of two-way reverse-time migration applications that utilize sharp boundaries in the migration velocity model to migrate multiply scattered arrivals (e.g., Fletcher et al., 2006; Guitton et al., 2006; Jones et al., 2007) rely on conventional migration practices and do not evaluate the volume integral term in the two-way imaging condition. Our approach for generating two-way reciprocity-based images can be implemented for imaging multiple-scattered arrivals using interpretation-based wavespeed models containing sharp discontinuities, i.e., by using sharp horizons picked from preexisting images and using our two-way formulation to adapt a reverse-time migration scheme. Likewise, our one-way nonlinear EI formulation based on multidimensional deconvolution is readily applicable to one-way migrations that rely on amplitude-preserving one-way extrapolators (e.g., Zhang et al., 2007) or to recursive one-way migrations that target imaging multiples (e.g., Berkhout and Verschuur, 2006; Malcolm et al., 2009).

CONCLUSIONS

EIs in wavefield seismic imaging can be defined explicitly as space- and time-dependent objects in the subsurface domain. In our case, we define EIs as time-varying scattered wavefields that are excited and acquired by virtual sources and receivers that surround a particular image point in the subsurface domain. This definition of an EI departs from the typical concept of a migrated image as a static representation of the discontinuities in the earth's subsurface. Two-way EIs are defined as scattered fields that satisfy the partial-differential equation for scattering in the subsurface domain, whereas we define one-way EIs as a dimensionless reflectivity operator that relates downgoing excitations with the upgoing subsurface waves recorded in the data.

Together with exact integral reciprocity relations, our definitions of one- and two-way EIs reveal an immediate connection between wave-equation imaging and the practice of seismic interferometry. Our extended images are, in fact, interferometric reconstructions of

one- and two-way scattering experiments that use model-dependent, depth-extrapolated data as opposed to physically observed recordings typical in seismic interferometry. Because we rely on the same general scattering reciprocity integrals used in interferometry to define EIs, we expect that our one- and two-way formulations for the extended imaging conditions account for nonlinear amplitude and multiple scattering effects.

To migrate multiples or to account for other nonlinear imaging effects, the computation of EIs departs significantly from today's practices in wave-equation migration. First, the depth-extrapolation step must be modified appropriately to model scattering interactions with model discontinuities — only for the receiver wavefields in two-way imaging and for source and receiver wavefields in the one-way case. Next, the imaging condition for two-way reciprocity EIs requires an additional scattering volume integral term that is not present in typical migration routines. In the one-way case, the extended imaging condition requires inversion of the full downgoing source-wavefield data matrix, which departs from current approaches that use cross-correlation or single-channel deconvolution.

Our explicit reciprocity-based descriptions of one- and two-way EIs can be used to address, analytically as well as numerically, the velocity-dependent signatures of these fully extended image gathers. Consequently, these wavefield-based EIs can help devise general formulations of image-domain objective functions for finite-frequency velocity inversion. In addition, one- and two-way EIs can be of immediate use in current reverse-time migration applications as well as in refining amplitude-preserving one-way wave-equation migration routines.

ACKNOWLEDGMENTS

We thank ION Geophysical/GXT Imaging Solutions (ION/GXT) for supporting this work and granting permission to publish it. P. Sava thanks the sponsors of the Center for Wave Phenomena consortium for financial support. I. Vasconcelos is thankful to Andrew Curtis (Edinburgh University) and David Halliday (Schlumberger) for sharing their material on source-receiver interferometry and imaging. We thank Kees Wapenaar, Jan Thorbecke, Sjoerd de Ridder, and an anonymous reviewer for their contributions in reviewing this paper.

REFERENCES

Bakulin, A., and R. Calvert, 2006, The virtual source method: Theory and case study: Geophysics, **71**, no. 4, SI139–SI150, doi: 10.1190/1.2216190.

Berkhout, A. J., 1982, Seismic migration, imaging of acoustic energy by wave field extrapolation, A: Theoretical aspects: Elsevier Scientific Publ. Co., Inc..

Berkhout, A. J., and D. J. Verschuur, 2006, Imaging of multiple reflections: Geophysics, **71**, no. 4, SI209–SI220, doi: 10.1190/1.2215359.

Beylkin, G., 1985, Imaging of discontinuities in the inverse scattering problem by inversion of a causal generalized Radon transform: Journal of Mathematical Physics, **26**, no. 1, 99–108, doi: 10.1063/1.526755.

Budreck, D. E., and J. H. Rose, 1990, Three-dimensional inverse scattering in anisotropic elastic media: Inverse Problems, **6**, no. 3, 331–348, doi: doi:10.1088/266-5611/6/3/004.

Campillo, M., and A. Paul, 2003, Long-range correlations in the diffuse seismic coda: Science, **299**, no. 5606, 547–549, doi: 10.1126/science.1078551.

Chauris, H., 2000, Analyse de vitesse par migration pour l' imagerie des structures complexes en sismique réflexion: Ph.D. dissertation, École des Mines de Paris.

Claerbout, J. F., 1968, Synthesis of a layered medium from its acoustic transmission response: Geophysics, **33**, 264–269, doi: 10.1190/1.1439927.

———, 1971, Toward a unified theory of reflector mapping: Geophysics, **36**, 467–481, doi: 10.1190/1.1440185.

———, 1985, Imaging the earth's Interior. Blackwell Scientific Publishers.

Clayton, R. W., and R. H. Stolt, 1981, A Born-WKBJ inversion method for acoustic reflection data: Geophysics, **46**, 1559–1567, doi: 10.1190/1.1441162.

Curtis, A., P. Gerstoft, H. Sato, R. Snieder, and K. Wapenaar, 2006, Seismic interferometry — Turning noise into signal: The Leading Edge, **25**, 1082–1092, doi: 1.1190/1.2349814.

Curtis, A., and D. Halliday, 2010, Source-receiver wavefield interferometry: Physical Review E: Statistical, Nonlinear, and Soft Matter Physics, **81**, no. 4, 046601, doi: 10.1103/PhysRevE.81.046601.

de Bruin, C. G. M., C. P. A. Wapenaar, and A. J. Berkhout, 1990, Angle-dependent reflectivity by means of prestack migration: Geophysics, **55**, 1223–1234, doi: 10.1190/1.1442938.

de Hoop, M. V., and A. T. de Hoop, 1999, Wave-field reciprocity and optimization in remote sensing: Proceedings of the Royal Society of London, 456, 641–682.

de Hoop, M. V., and A. K. Gautesen, 2003, Uniform asymptotic expansion of the square-root Helmholtz operator and the one-way wave propagator: SIAM Journal of Applied Mathematics, **63**, 777–800.

de Hoop, M. V., R. van der Hilst, and P. Shen, 2006, Wave-equation reflection tomography: Annihilators and sensitivity kernels: Geophysical Journal International, **167**, 1332–1352, doi: 10.1111/j.1365-246X.2006.03132.x.

Esmersoy, C., and M. Oristaglio, 1988, Reverse-time wave-field extrapolation, imaging and inversion: Geophysics, **53**, 920–931, doi: 10.1190/1.1442529.

Fink, M., 1997, Time-reversed acoustics: Physics Today, **50**, no. 3, 34–40, doi: 10.1063/1.881692.

Fishman, L., and J. J. McCoy, 1984, Derivation and application of extension of parabolic wave theories. I. The factorized Helmholtz equation: Journal of Mathematical Physics, **25**, no. 2, 285–296, doi: 10.1063/1.526149.

Fishman, L., J. J. McCoy, and S. C. Wales, 1987, Factorization and path integration of the Helmholtz equation: Numerical algorithms: Journal of the Acoustical Society of America, **81**, no. 5, 1355–1376, doi: 10.1121/1.394542.

Fletcher, R. P., P. J. Fowler, P. Kitchenside, and U. Albertin, 2006, Suppressing unwanted internal reflections in prestack reverse-time migration: Geophysics, **71**, no. 6, E79–E82, doi: 10.1190/1.2356319.

Fokkema, J. T., and P. M. van den Berg, 1993, Seismic applications of acoustic reciprocity: Elsevier Scientific Publ. Co., Inc.

Guitton, A., B. Kaelin, and B. Biondi, 2006, Least-square attenuation of reverse time migration artifacts: 76th Annual International Meeting, SEG, Expanded Abstracts, 2348–2352.

Halliday, D., and A. Curtis, 2010, An interferometric theory of source-receiver scattering and imaging: Geophysics, **75**, this issue.

Hansen, P. C., 1997, Rank-deficient and discrete ill-posed problems: Numerical aspects of linear inversion: SIAM.

Jones, I., M. C. Goodwin, I. D. Berranger, H. Zhou, and P. Farmer, 2007, Application of anisotropic 3D reverse time migration to complex North Sea imaging: 77th Annual International Meeting, SEG, Expanded Abstracts, 2140–2144.

Malcolm, A. E., B. Ursin, and M. V. de Hoop, 2009, Seismic imaging and illumination with internal multiples: Geophysical Journal International, **176**, 847–864, doi: 10.1111/j.1365-246X.2008.03992.x.

Mulder, W., 2005, Rigorous redatuming: Geophysical Journal International, **161**, 401–415, doi: 10.1111/j.1365-246X.2005.02615.x.

Mulder, W., and A. ten Kroode, 2002, Automatic velocity analysis by differential semblance optimization: Geophysics, **67**, 1184–1191, doi: 10.1190/1.1500380.

Oristaglio, M., 1989, An inverse scattering formula that uses all the data: Inverse Problems, **5**, no. 6, 1097–1105, doi: 10.1088/0266-5611/5/6/015.

Plessix, R. E., 2006, A review of the adjoint-state method for computing the gradient of a functional with geophysical applications: Geophysical Journal International, **167**, 495–503, doi: 10.1111/j.1365-246X.2006.02978.x.

Pratt, R. G., 1999, Seismic waveform inversion in the frequency domain, Part 1: Theory and verification in a physical scale model: Geophysics, **64**, 888–901, doi: 10.1190/1.1444597.

Prosser, R. T., 1969, Formal solutions to inverse scattering problems: Journal of Mathematical Physics, **10**, 1819–1822, doi: 10.1063/1.1664766.

Ramírez, A. C., and A. B. Weglein, 2009, Greens theorem as a comprehensive framework for data reconstruction, regularization, wavefield separation, seismic interferometry, and wavelet estimation: A tutorial: Geophysics, **74**, no. 6, W35–W62, doi: 10.1190/1.3237118.

Rickett, J. E., and J. F. Claerbout, 1999, Acoustic daylight imaging via spectral factorization; helioseismology and reservoir monitoring: The Leading Edge, **18**, 957–960, doi: 10.1190/1.1438420.

Rickett, J. E., and P. C. Sava, 2002, Offset and angle-domain common image-point gathers for shot-profile migration: Geophysics, **67**, no. 3, 883–889, doi: 10.1190/1.1484531.

Rose, J. H., M. Cheney, and B. DeFacio, 1985, Three dimensional inverse scattering: Plasma and variable velocity wave equations: Journal of Mathematical Physics, **26**, 2803–2813, doi: 10.1063/1.526705.

Sava, P., and B. Biondi, 2004, Wave-equation migration velocity analysis —

I: Theory: Geophysical Prospecting, **52**, 593–606, doi: 10.1111/j.1365-2478.2004.00447.x.
Sava, P., and S. Fomel, 2003, Angle-domain common-image gathers by wavefield continuation methods: Geophysics, **68**, 1065–1074, doi: 10.1190/1.1581078.
——–, 2006, Time-shift imaging condition in seismic migration: Geophysics, **71**, no. 6, S209–S217, doi: 10.1190/1.2338824.
Sava, P., and I. Vasconcelos, 2010, Extended imaging conditions for wave-equation migration: Geophysical Prospecting, **59**, doi: 10.1111/j.1365-2478.2010.00888.x.
Schuster, G. T., J. Yu, J. Sheng, and J. Rickett, 2004, Interferometric/daylight seismic imaging: Geophysical Journal International, **157**, 838–852, doi: 10.1111/j.1365-246X.2004.02251.x.
Shubin, M. A., 1987, Pseudodifferential operators and spectral theory: Springer-Verlag Berlin.
Sirgue, L., and R. G. Pratt, 2004, Efficient waveform inversion and imaging: A strategy for selecting temporal frequencies: Geophysics, **69**, no. 1, 231–248, doi: 10.1190/1.1649391.
Stolt, R. H., and A. B. Weglein, 1985, Migration and inversion of seismic data: Geophysics, **50**, 2458–2472, doi: 10.1190/1.1441877.
Symes, W. W., 2008, Migration velocity analysis and waveform inversion: Geophysical Prospecting, **56**, 765–790, doi: 10.1111/j.1365-2478.2008.00698.x.
——–, 2009, The seismic reflection inverse problem: Inverse Problems, **25**, no. 12, 123008, doi: 10.1088/0266-5611/25/12123008.
Tape, C., Q. Liu, A. Maggi, and J. Tromp, 2009, Adjoint tomography of the southern California crust: Science, **325**, no. 5943, 988–992, doi: 10.1126/science.1175298.
Tarantola, A., 1984, Inversion of seismic reflection data in the acoustic approximation: Geophysics, **49**, 1259–1266, doi: 10.1190/1.1441754.
Thorbecke, J., 1997, Common focus point technology: Ph.D. dissertation, Delft University of Technology.
Thorbecke, J., and A. J. Berkhout, 2006, Recursive prestack depth migration using CFP gathers: Geophysics, **71**, no. 6, S273–S283, doi: 10.1190/1.2348517.
Thorbecke, J., and K. Wapenaar, 2007, On the relation between seismic interferometry and the migration resolution function: Geophysics, **72**, no. 6, T61–T66, doi: 10.1190/1.2785850.
van Manen, D.-J., A. Curtis, and J. O. A. Robertsson, 2006, Interferometric modeling of wave propagation in inhomogeneous elastic media using time-reversal and reciprocity: Geophysics, **71**, no. 4, SI47–SI60, doi: 10.1190/1.2213218.
van Manen, D.-J., J. O. A. Robertsson, and A. Curtis, 2005, Modeling of wave propagation in inhomogeneous media: Physical Review Letters, **94**, no. 16, 164301, doi: 10.1103/PhysRevLett.94.164301.
Vasconcelos, I., 2008, Generalized representations of perturbed fields-applications in seismic interferometry and migration: 78th Annual International Meeting, SEG, Expanded Abstracts, 2927–2941.
Vasconcelos, I., P. Sava, and H. Douma, 2009a, Wave-equation extended images via image-domain interferometry: 79th Annual International Meeting, SEG, Expanded Abstracts, 2839–2843.
Vasconcelos, I., and R. Snieder, 2008, Interferometry by deconvolution, Part 1: Theory for acoustic waves and numerical examples: Geophysics, **73**, no. 3, S115–S128, doi: 10.1190/1.2904554.
Vasconcelos, I., R. Snieder, and H. Douma, 2009b, Representation theorems and Greens function retrieval for scattering in acoustic media: Physical Review E: Statistical, Nonlinear, and Soft Matter Physics, 80, no. 3, 036605, doi: 10.1103/PhysRevE.80.036605.
Wapenaar, K., 2004, Retrieving the elastodynamic Green's function of an arbitrary inhomogeneous medium by cross correlation: Physical Review Letters, **93**, no. 25, 254301, doi: 10.1103/PhysRevLett.93.254301.
——–, 2006, Green's function retrieval by cross-correlation in case of one-sided illumination: Geophysical Research Letters, **33**, no. 19, L19304, doi: 10.1029/2006GL027747.
——–, 2007, General representations for wavefield modeling and inversion in geophysics: Geophysics, **72**, no. 5, SM5–SM17, doi: 10.1190/1.2750646.
Wapenaar, C. P. A., M. W. P. Dillen, and J. T. Fokkema, 2001, Reciprocity theorems for electromagnetic or acoustic one-way wave fields in dissipative inhomogeneous media: Radio Science, **36**, no. 5, 851–863, doi: 10.1029/2000RS002394.
Wapenaar, K., D. Draganov, and J. Robertsson, 2006, Introduction to the supplement on seismic interferometry: Geophysics, **71**, no. 4, SI1–SI4, doi: 10.1190/1.2352998.
Wapenaar, K., and J. Fokkema, 2006, Green's function representations for seismic interferometry: Geophysics, **71**, no. 4, SI33–SI46, doi: 10.1190/1.2213955.
Wapenaar, C. P. A., G. L. Peels, V. Budejicky, and A. J. Berkhout, 1989, Inverse extrapolation of primary seismic waves: Geophysics, **54**, 853–863, doi: 10.1190/1.1442714.
Wapenaar, K., E. Slob, and R. Snieder, 2008, Seismic and electromagnetic controlled-source interferometry in dissipative media: Geophysical Prospecting, **56**, no. 3, 419–434, doi: 10.1111/j.1365-2478.2007.00686.x.
Wapenaar, K., E. Slob, A. Curtis, and R. Snieder, 2010, Tutorial on seismic interferometry, Part II: Underlying theory and new advances: Geophysics, **75**, this issue.
Wapenaar, K., J. Thorbecke, and D. Draganov, 2004, Relations between reflection and transmission responses of three-dimensional inhomogeneous media: Geophysical Journal International, **156**, no. 2, 179–194, doi: 10.1111/j.1365-246X.2003.02152.x.
Weaver, R. L., and O. I. Lobkis, 2001, Ultrasonics without a source: Thermal fluctuation correlations at MHz frequencies: Physical Review Letters, **87**, no. 13, 134301, doi: 10.1103/PhysRevLett.87.134301.
Weglein, A. B., F. V. Araújo, P. M. Carvalho, R. H. Stolt, K. H. Matson, R. T. Coates, D. Corrigan, D. J. Foster, S. A. Shaw, and H. Zhang, 2003, Inverse scattering series and seismic exploration: Inverse Problems, **19**, no. 6, R27–R83, doi: 10.1088/0266-5611/19/6/R01.
Zhang, Y., S. Xu, N. Bleistein, and G. Zhang, 2007, True-amplitude, angle-domain, common-image gathers from one-way wave-equation migrations: Geophysics, **72**, no. 1, S49–S58, doi: 10.1190/1.2399371.
Zhu, H., Y. Luo, T. Nissen-Meyer, C. Morency, and J. Tromp, 2009, Elastic imaging and time-lapse migration based on adjoint methods: Geophysics, **74**, no. 6, WCA167–WCA177.